Cell Reports
Physical Science

CellPress
OPEN ACCESS

Article

Interexciton nonradiative relaxation pathways in the peridinin-chlorophyll protein

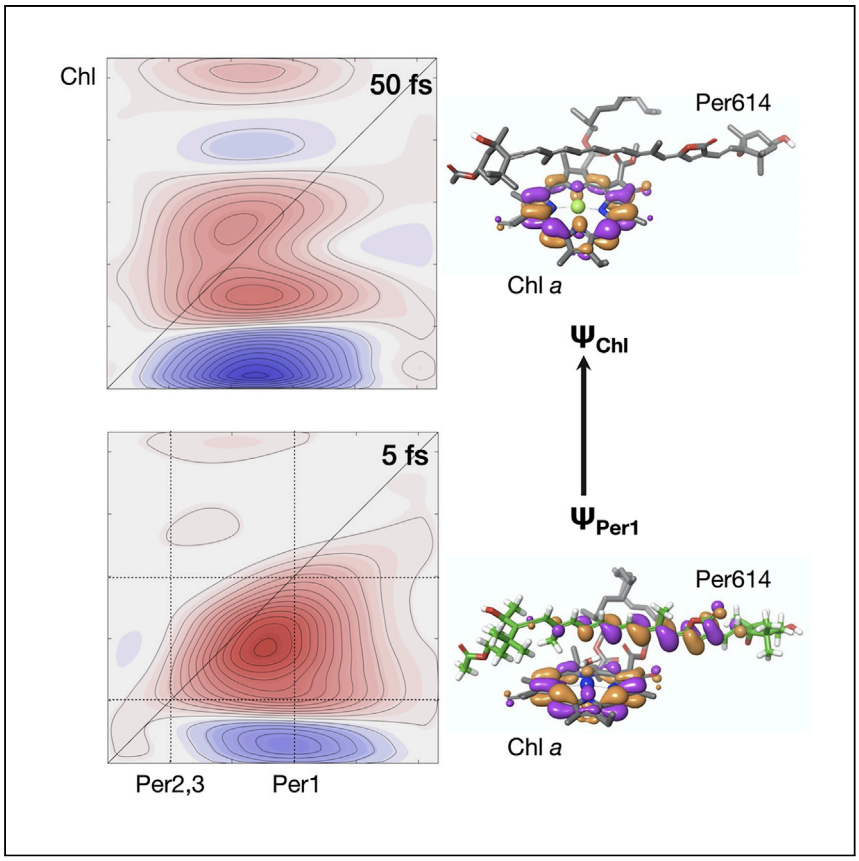

Tilluck et al. reveal how excitation energy transfer in the peridinin-chlorophyll protein from marine dinoflagellates involves quantum coherent mixing of the excited states of the clustered chromophores in each protein domain. The results suggest that solar photons might be captured efficiently in photocatalytic devices and solar cells by delocalized nanomaterials.

Ryan W. Tilluck, Soumen Ghosh, Matthew J. Guberman-Pfeffer, ..., Harry A. Frank, José A. Gascón, Warren F. Beck

beckw@msu.edu

HIGHLIGHTS

A two-step pathway transfers energy from peridinin excitons to chlorophylls

Excitation energy is trapped by chlorophyll acceptors in less than 50 fs

Delocalization collapses as excitation progresses irreversibly down the pathway

Transfer rates are robust when chlorophyll *a* is replaced with chlorophyll *b*

Tilluck et al., Cell Reports Physical Science 2, 100380
March 24, 2021
https://doi.org/10.1016/j.xcrp.2021.100380

Cell Reports
Physical Science

CellPress
OPEN ACCESS

Article

Interexciton nonradiative relaxation pathways in the peridinin-chlorophyll protein

Ryan W. Tilluck,[1] Soumen Ghosh,[2] Matthew J. Guberman-Pfeffer,[3,4] Jerome D. Roscioli,[1,5] J.K. Gurchiek,[1] Amy M. LaFountain,[3,6] Harry A. Frank,[3] José A. Gascón,[3] and Warren F. Beck[1,7,*]

SUMMARY

Excitation energy transfer can be unusually efficient and structurally robust when mediated by molecular excitons, which arise in a photosynthetic light-harvesting protein when delocalized excitations of the electronic chromophores are created upon absorption of light. Here we report results from two-dimensional electronic spectroscopy and electronic structure calculations, revealing that excitation energy is transferred between the peridinin and chlorophyll excitons in the peridinin-chlorophyll protein from marine dinoflagellates over a delocalized, two-step pathway. Upon absorption of light by the peridinins in the strong, mid-visible absorption band, excitation energy is trapped by the chlorophylls in less than 50 fs at room temperature. The overall process is slowed only by a few fs upon replacement of chlorophyll *a* with chlorophyll *b*. The key step in the pathway transfers excitation from higher-energy peridinin excitons with more extensive delocalization to the lowest-energy peridinin exciton, which is delocalized only over peridinin 614 and the neighboring chlorophyll.

INTRODUCTION

Photosynthetic organisms incorporate light-harvesting pigment-protein complexes to absorb incident solar photons and transfer a fraction of the captured excitation energy from them to reaction center complexes, where the energy is stored as a transmembrane electrochemical gradient by fast electron transfer reactions.[1] In a number of well-characterized examples, absorption of light instantaneously creates molecular excitons, collective excitations of pairs or larger clusters of the chromophores in a protein. Excitons result from quantum coherent mixing of the electronic states of the individual chromophores because of the presence of strong electronic interactions between them.[2,3] Excitation energy is then relayed in less than 50 fs in some cases to the lowest-energy exciton states of the cluster, which are derived mainly from the red-shifted terminal emitter chromophores that provide an interface to the adjacent reaction centers. Similar interexciton nonradiative relaxation processes are observed in the primary electron donor of purple bacterium reaction centers, which is a strongly coupled pair of bacteriochlorophyll (BChl) molecules,[4] and, for example, in a model system consisting of pairs of diacetylene-linked perylenediimide molecules.[5] A central question here is how the structure of a light-harvesting protein or material is able to sustain delocalization over a set of chromophores long enough that the excitation energy efficiently reaches the lowest-energy excitons despite the natural tendency for it to collapse onto a given chromophore.[6] Excitation energy would then hop incoherently and much more slowly, typically in a few picoseconds, from one chromophore to another via the Förster mechanism.[7]

[1]Department of Chemistry, Michigan State University, 578 S. Shaw Lane, East Lansing, MI 48824, USA

[2]Department of Physics, Politecnico di Milano, Milan, Italy

[3]Department of Chemistry, University of Connecticut, 55 North Eagleville Road, Storrs, CT 06269, USA

[4]Present address: Department of Chemistry, Yale University, 225 Prospect Street, New Haven, CT 06511, USA

[5]Present address: The Dow Chemical Company, Midland, MI 48674, USA

[6]Present address: Department of Ecology and Evolutionary Biology, 75 North Eagleville Road, Storrs, CT 06269-3043, USA

[7]Lead contact

*Correspondence: beckw@msu.edu

https://doi.org/10.1016/j.xcrp.2021.100380

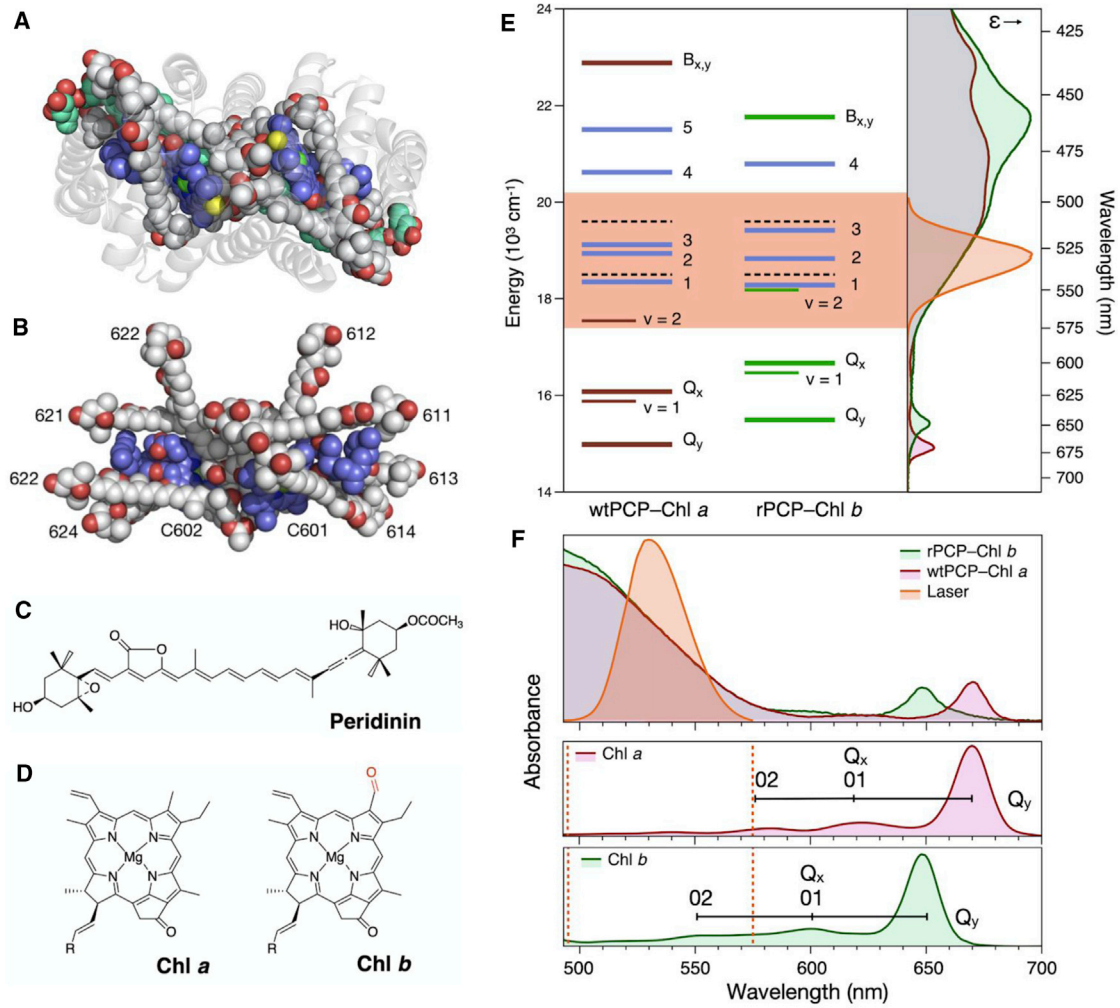

Figure 1. Structure and linear absorption spectroscopy of PCP complexes

(A) Structure of rPCP-Chl *b* (PDB: 2X20),[23] viewed along the 2-fold symmetry axis.

(B) Structure of the chromophore cluster in rPCP-Chl *b*, with the symmetry axis oriented vertically. The chromophores are numbered as in the crystal structure.[10]

(C and D) Structures of peridinin, Chl *a*, and Chl *b*, with the formyl oxygen of the latter marked in red.

(E) Energy level diagram, with corrections from that of Roscioli et al.,[13] showing the peridinin (blue), Chl *a* (purple), and Chl *b* (green) optical transition frequencies for the wtPCP-Chl *a* and rPCP-Chl *b* complexes determined from spectral deconvolution of linear absorption spectra at 10 K.[24,26] The numbered peridinin energy levels correspond to the S_0 ($v = 0$) → S_2 ($v = 0$) vibronic transitions for the per1–per4 excitons (and per5 for wtPCP-Chl *a*). The Chl levels are labeled $B_{x,y}$, Q_x, and Q_y for each complex; the Q_y $v = 1$ and $v = 2$ vibrational levels are estimated from the spectra in (F). Dashed lines indicate the center wavelengths of the excitation regions selected for global modeling of the 2DES responses from the per2,3 and per1 excitons.

(F) Room-temperature (23°C) absorption spectra from wtPCP-Chl *a* (purple bands) and rPCP-Chl *b* (green bands), with the laser excitation spectrum (orange band) superimposed, compared with the absorption spectra of five-coordinate Chl *a* (red) and Chl *b* (green).[27] The vibronic structure is labeled for the Q_y band; the Q_x band (00, for S_0 [$v = 0$] → S_1 [$v = 0$]) coincides approximately with the Q_y 01 (S_0 [$v = 0$] → S_1 [$v = 1$]) band in five-coordinate Chls.[28] The orange dashed lines mark the actual detection axis limits for the 2DES spectra (Figures 2 and 3).

Here we report the results of a two-dimensional electronic spectroscopy (2DES)[8] and electronic structure calculation study of the ultrafast excitation energy transfer mechanisms in the peridinin-chlorophyll protein (PCP) from marine dinoflagellates. PCP is a water-soluble, peripheral light-harvesting complex that absorbs strongly in the mid-visible, 470- to 550-nm wavelength range. It relays the excitation energy it captures principally to the photosystem II reaction center via membrane-bound chlorophyll proteins.[9] The structure of the PCP complex (Figures 1A and 1B) is a

2-fold symmetric, two-domain assembly, with each domain consisting of a basket of α helices containing four peridinin carotenoids (Figure 1C) clustered tightly around a single chlorophyll (Chl) (Figure 1D).[10] This arrangement is distinctive because the chromophore clusters resemble nanocrystals, lacking any intervening protein-derived scaffolding. Several recent investigations have established that excitation energy transfer to the Chl *a* acceptors in PCP complexes occurs in less than 20 fs when peridinins absorbing in the long-wavelength onset of the mid-visible absorption band are photoexcited.[11–14] These ultrafast processes are consistent with an assignment to internal conversion processes between molecular excitons, but electronic structure calculations indicate that only a modest degree of delocalization occurs over the peridinin-Chl cluster in each protein domain.[15–17] Assignment of PCP to the strong electronic coupling regime has been suggested early in the studies, with femtosecond pump-probe and fluorescence line-narrowing spectroscopy by Zigmantas et al.[18] and Kleima et al.,[19] respectively. The recent heterodyne transient grating measurements in our laboratory[11] led us to suggest that the yield of the ultrafast excitation energy transfer processes in PCP is limited kinetically by competition with a nonradiative decay pathway by the peridinins, from the S_2 state prepared by absorption of a photon to a localized intermediate state we labeled S_x, which could then serve as the donor for the Förster energy transfer processes. Others have assigned this peridinin intermediate state to the S_1 state proper and/or to a form of the S_1 state with strong intramolecular charge transfer (ICT) properties.[18,20]

The details of the ultrafast excitation transfer and nonradiative decay processes can be examined with unusual clarity using 2DES by comparing the wild-type complexes containing Chl *a* acceptors (wtPCP-Chl *a*) with reconstituted complexes containing Chl *b* (rPCP-Chl *b*),[21,22] which are constructed using a polypeptide sequence taken from the N-terminal domain of the PCP structure. When reconstituted with pigments, rPCP-Chl *b* assembles a 2-fold symmetric dimer complex[21] (Figures 1A and 1B) with almost exactly the same X-ray crystal structure[13,23] as that for the naturally occurring, heterodimer PCP complex.[10] In aqueous solution, wtPCP-Chl *a* forms trimeric aggregates, whereas rPCP-Chl *b* remains monomeric. At cryogenic temperatures, the absorption spectra of the natural and reconstituted complexes nevertheless contain a very similar pattern of four peridinin transitions (Figure 1E). A fifth, higher-energy peridinin absorption transition in wtPCP-Chl *a* is currently attributed to splitting of the principal exciton levels by the symmetry-breaking electrostatic differences between the N- and C-terminal domains[24] and by the long-range interchromophore electronic couplings across the two domains.[25] Figure 1F shows that replacement of Chl *a* with Chl *b* changes the energy gaps from the peridinin energy levels to the vibronic energy levels of the Chls in the two complexes because the Chl *b* levels are shifted by several hundred wavenumbers to the blue of those from Chl *a*.

In the present study, we perform 2DES experiments on the wtPCP-Chl *a* and rPCP-Chl *b* complexes combined with electronic structure calculations to determine the pathway and mechanism that transfers excitation energy to the Chl acceptors when absorption transitions in the main absorption band prepare peridinin excitons per1–per3 (Figure 1E). The 2DES spectra allow determination in parallel[8] of the responses that follow direct optical excitations of the peridinin excitons at different transition wavelengths. The spectra of the excitation pulses partially overlap, however, with transitions to the Q_y $v = 1$ and $v = 2$ levels, so the arrival of excitation energy at the Chl acceptors can be detected in both complexes. Global and target modeling establishes that the per1 exciton serves as an intermediate state populated by fast interexciton relaxation from the per2 and per3 excitons. As this process

occurs, the delocalized excitation initially present in the peridinin-Chl cluster collapses, yielding a localized excitation on the Chl acceptor in less than 50 fs.

RESULTS

Linear spectroscopy and chromophore assignments in the PCP complexes

2DES experiments with room-temperature (23°C) samples of the wtPCP-Chl *a* and rPCP-Chl *b* complexes were carried out with a newly constructed spectrometer (Supplemental experimental procedures; Note S1) employing adaptive pulse shapers to compress the laser pulses and prepare and scan the coherence time interval τ in the excitation pulse sequence (pulse 1-τ-pulse 2) required for the three-pulse stimulated photon-echo experiment[8] using a two-beam, pump-probe configuration.[29] To excite the per1–per3 peridinin excitons in the mid-visible absorption band (Figures 1E and 1F), the laser spectrum (530 nm, 15-fs pulses) was tuned farther to the blue than in our previous work.[12,13] Calculations indicate that the per2 and per3 excitons are located predominantly on peridinin chromophores 611 and 613, respectively, whereas per1 is principally on peridinin 614 (Figure 1B).[17,25] These chromophore assignments are in agreement with those of Ilagan et al.,[24] who identified the contribution of peridinin 614 via site-directed mutagenesis. Because the per2 and per3 transitions are effectively degenerate in wtPCP-Chl *a* (Figure 1E) and are not resolved in the 2DES experiments, hereafter we refer to them together as per2,3. The red tail of the laser spectrum spans the 560- to 575-nm onset of the partially resolved 0–2 absorption transition of the Q_y absorption band of Chl *a* in wtPCP-Chl *a* complexes (Figures 1E and 1F). In the rPCP-Chl *b* complexes, the center of the 0–2 transition of Q_y for Chl *b* is blue shifted to 550 nm, whereas the onset of the 0–1 transition is at the red edge of the laser spectrum above 570 nm.

Cross-peaks in 2DES spectra report excitation energy transfer in PCP complexes

Figures 2 and 3 compare a set of 2DES spectra from the wtPCP-Chl *a* and rPCP-Chl *b* complexes at 23°C with the waiting times (T) between the second and third excitation pulses selected over the 5- to 500-fs range. Note S2 is related to Videos S1 and S2, which are assembled from the full set of spectra acquired over the waiting time T = 0 fs–300 ps range. Each spectrum was obtained as the average from that acquired in nine τ scans. The amplitudes plotted in Figures 2 and 3 are normalized with respect to that of the global maximum in the entire (τ,T) dataset, whereas each spectrum in Videos S1 and S2 is autoscaled separately to reveal additional detail.

By inspecting the 2DES spectra from the PCP complexes shown in Figures 2 and 3, one can identify several features arising from excitation energy transfer.

1. At short T, the 2DES spectra exhibit positive-going ground-state bleaching (GSB) and stimulated emission (SE) signals along the diagonal. As indicated in Figures 1E and 1F, these signals arise principally from photoexcitation of the per1–per3 excitons over the 495- to 560-nm range, but the vibronic transitions of the Chl acceptors increasingly contribute at longer wavelengths. The GSB and SE signals are broadened extensively with respect to the antidiagonal direction by electronic dephasing even at short T.
2. Negative-going excited-state absorption (ESA) signals are observed initially below the diagonal (to shorter detection wavelengths) but increasingly above the diagonal (to longer detection wavelengths) at longer T in both complexes. ESA signals have been characterized extensively from peridinin in solution and in PCP complexes,[18,20] and the kinetics observed here are essentially identical

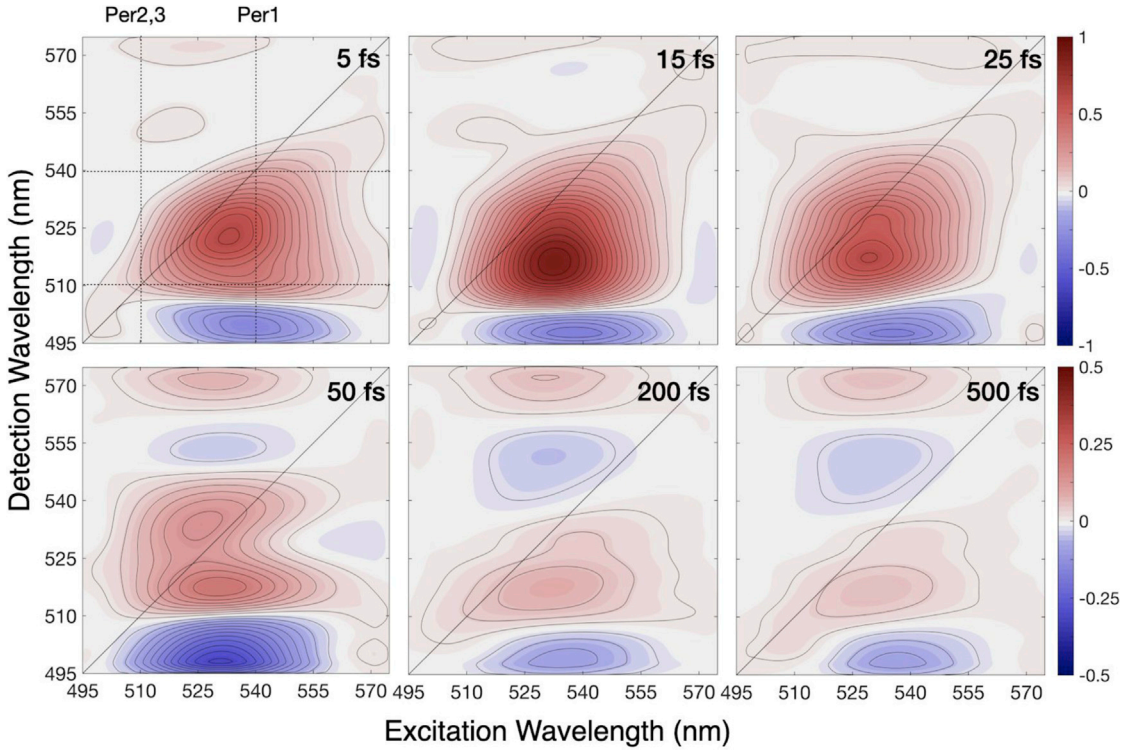

Figure 2. 2DES spectra from wtPCP-Chl *a* complexes
Spectra were recorded at 23°C over the waiting time (*T*) = 5- to 500-fs range.

to that detected previously in one-dimensional heterodyne transient grating experiments.[11]

3. Excitation energy transfer processes are reported by formation of positive-going cross-peaks above the diagonal and by decay of the diagonal GSB and SE signals as excitation energy flows from the per2 or per3 excitons to the per1 exciton and then to the Chl acceptor in less than 50 fs in both complexes. The main difference between the 2DES spectra from wtPCP-Chl *a* and rPCP-Chl *b* involves the Chl cross-peaks above 565 nm along the detection axis. In the wtPCP-Chl *a* spectra (Figure 2), a cross-peak develops at the blue edge of the $v = 2$ transition of Q_y for Chl *a*. The cross-peak in the rPCP-Chl *b* spectra is red shifted to the edge of the spectrum compared with that from wtPCP-Chl *a*, which suggests an assignment to the $v = 1$ transition of Q_y for Chl *b* rather than to the $v = 2$ transition, whose peak lies well to the blue of that for Chl *a*.

Global and target modeling of the 2DES spectra from PCP complexes resolves an ultrafast excitation transfer pathway in PCP complexes

The responses initiated by optical excitations of the per2,3 or per1 excitons in the wtPCP-Chl *a* and rPCP-Chl *b* complexes were isolated from the 2DES spectra and modeled separately using global and target modeling[30] with the CarpetView package (Light Conversion). This approach models the response driven by a specific optical excitation as a linear combination of the evolution-associated difference spectra (EADS) for each of the spectrokinetic species in the scheme shown in Figure 4A, as scaled by their time-dependent populations. Figures 4B, 5, and 6 describe the global model for the per2,3 excitation in the wtPCP-Chl *a* complex. Figure S9 includes similar figures to report the global model for the per1 excitation. Figures S10 and S11 document the

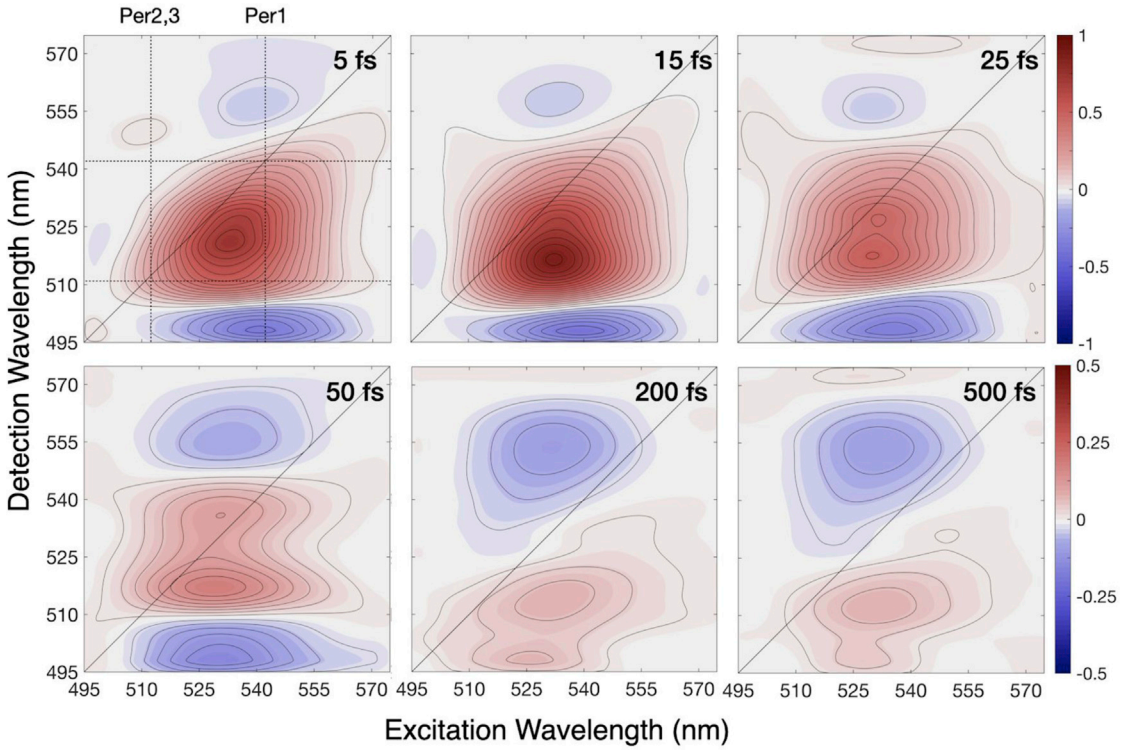

Figure 3. 2DES spectra from rPCP-Chl *b* complexes
Spectra were recorded at 23°C over the T = 5- to 500-fs range.

global models for the per2,3 and per1 excitations in rPCP-Chl *b*, which share many of the details of those in wtPCP–Chl *a*. Additional coverage of the methods used and the results obtained with simpler global models, which were used to test aspects of the kinetic scheme, are reported in Notes S3 and S4 and Figures S4–S8.

The first result from the global and target analysis of the 2DES spectra in both PCP complexes is that a two-step ultrafast excitation transfer pathway is observed after optical excitation of the per2,3 excitons. This pathway is shown in Figure 4A as the left vertical column of states. The results from preliminary models lacking the per2,3-to-per1 step (Figures S7 and S8) establish that the per2,3 and per1 responses are resolved kinetically and spectrally. The per1 exciton serves as an intermediate, accepting excitation from per2,3 in 10 fs and relaying it to the Chl acceptors in 25 fs (Figures 4B and 5). The excitation transfer times returned by the global models for the decay of the per2,3 and per1 excitations in rPCP-Chl *b*, 13 fs and 28 fs, respectively, are longer than those in wtPCP-Chl *a* but only by a few femtoseconds (Table 1). About a third of the peridinin-excited states decay nonradiatively to yield S_x, which transfers excitation energy to the Chl′ compartment in the kinetic scheme via the Förster mechanism. An additional discussion of the nonradiative branch of the kinetic scheme and of possible assignments for the S_x state is provided in Note S5.

A comparison of the EADS corresponding to instantaneous excitation of the per2,3 and per1 excitons in the wtPCP-Chl *a* and rPCP-Chl *b* complexes (Figures 6 and S9–S11) indicates the presence of delocalized excitations in the peridinin-Chl cluster in the PCP complexes. The positive-going net GSB/SE character centered at 520 nm in the EADS for the per2,3 excitation (Figures 6 and S10) is overlapped by an underlying broader region of negative-going ESA extending to the blue and red. The net

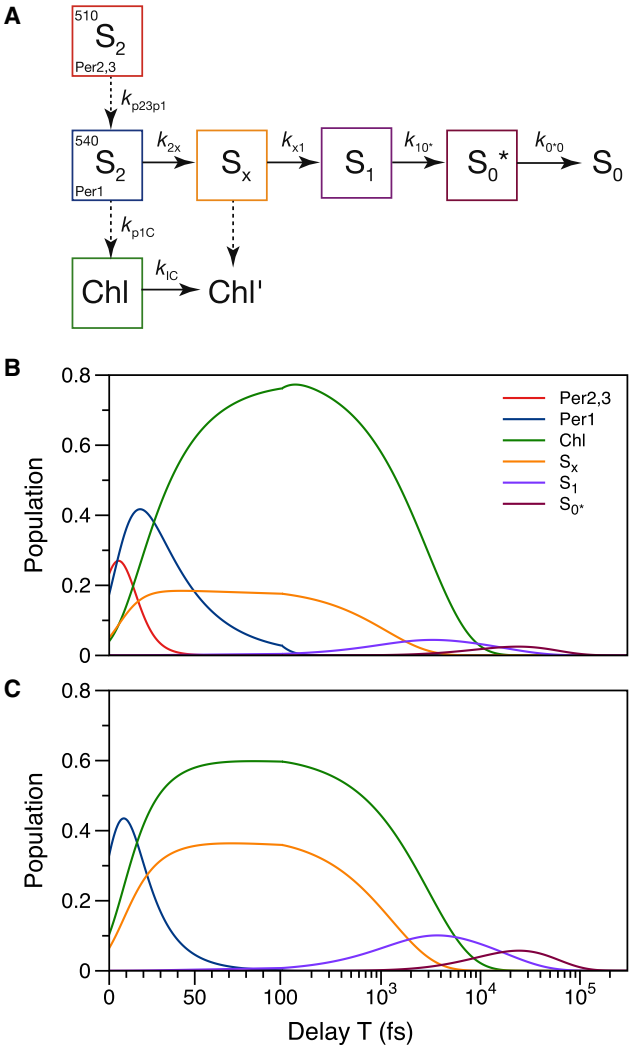

Figure 4. Kinetic scheme and time evolution of the population in the global and target models for the 2DES spectra from the wtPCP-Chl *a* and rPCP-Chl *b* complexes

(A) The kinetic scheme shows the pathways of excitation energy transfer (dotted arrows) and nonradiative decay (solid arrows) following excitation of the per2,3 exciton.

(B and C) The populations of the spectrokinetic species determined in the optimized models for optical excitation of (B) the per2,3 and (C) the per1 excitons in wtPCP-Chl *a* are plotted with respect to semilogarithmic time axes, with the linear section extending to 100 fs. The scaling of the population axes corresponds to that in the 2DES spectra (Figure 2). Figures S10 and S11 show the corresponding responses in rPCP-Chl *b* complexes. The time constants obtained in the optimized global models for both complexes are compared in Table 1.

negative signal character largely disappears in the EADS from per1 when populated as an intermediate or when excited directly optically (Figures S9 and S11). In addition to GSB and SE transitions, the exciton states for a chromophore cluster exhibit ESA transitions accessing doubly excited exciton states. As the delocalization collapses in a chromophore cluster, these ESA transitions disappear because the doubly excited states vanish.[31,32] The EADS for the Chl acceptor (Figures 6 and S9–S12) has a relatively weak region of negative-going ESA in the blue overlapping with a sharper net positive region from net GSB/SE above 545 nm for wtPCP-Chl *a* and above 535 nm for rPCP-Chl *b*, which overlaps with the Chl Q_y vibronic structure in the red part of the laser spectrum (Figures 1E and 1F). Given the decay of the diagonal

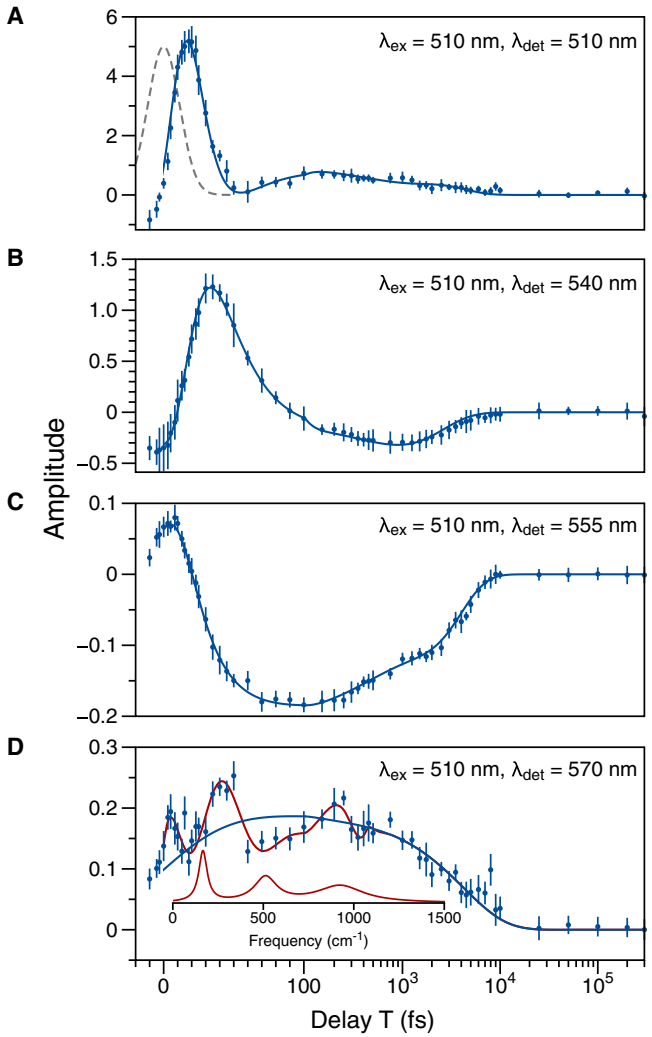

Figure 5. Amplitude transients after optical excitation of the per2,3 excitons in wtPCP-Chl *a*

(A–D) The amplitude detected at (A) 510 nm, (B) 540 nm, (C) 555 nm, and (D) 570 nm in the 2DES spectrum (Figure 2) is superimposed in each panel with that obtained from the global model (smooth curves) as a function of *T*, which is plotted against a semilogarithmic axis split at 100 fs. The bars on each plotted data point report 95% confidence intervals for the amplitudes. (A) includes a dashed, 21-fs Gaussian showing the instrument-response function used in the global model, which is convoluted with the responses from the spectrokinetic species. In (D), the amplitude is plotted superimposed with a red curve showing a fit of the residual (signal − global model) to a rising, sum of damped cosinusoids function. The model parameters are listed in Table S5. The inset shows the frequency spectrum corresponding to the amplitude of the modulation components.

regions of the 2DES spectra that accompanies the less than 50-fs rise of population for the Chl acceptor in the global models, the Chl EADS should be assigned to a predominantly localized excitation because a shared ground state with the peridinin excitons does not persist.

In the 2DES spectra from wtPCP-Chl *a* (Figure 2), formation of a cross-peakabove 565 nm is consistent with a SE signal from a population deposited in the Q_y $v = 2$ vibronic band of Chl *a* (Figure 1F). As noted above, a weaker cross-peak from the Chl acceptor in rPCP-Chl *b* (Figure 3) is observed at detection wavelengths above 570 nm (the cross-peaks are more prominent in Videos S1 and S2, related to Note

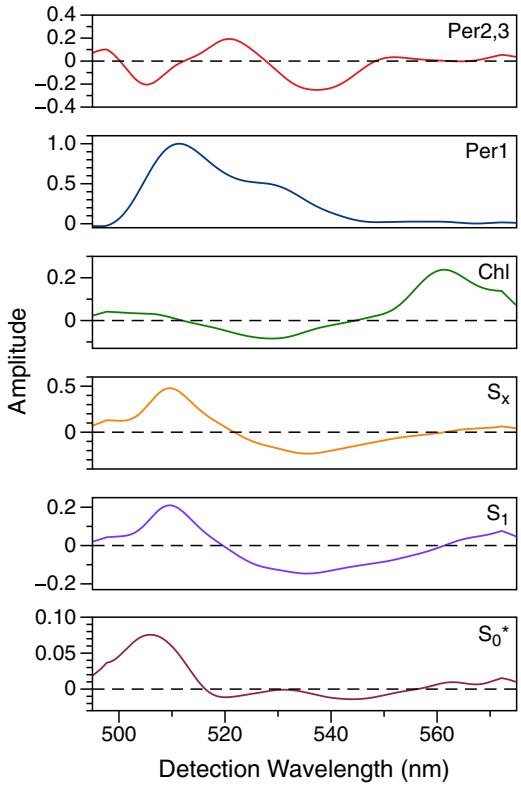

Figure 6. Evolution-associated difference spectra (EADS) for the global model for the per2,3 excitation in the wtPCP-Chl *a* complex

S2). Given that the peridinin transitions are very similar in the two complexes, these observations suggest that the $v = 1$ level of Q_y receives the excitation in the Chl *b* case instead of $v = 2$, which is almost degenerate with per1. In both complexes, 90% of the rise in population at the Chl acceptors is observed in less than 50 fs, and the maximum amplitude of the Chl cross-peaks is reached in the 90- to 100-fs range. The transients detected at the Chl cross-peak (Figures 5D and S12) exhibit relatively deep amplitude modulations. A definitive assignment of these modulated signals will require a subsequent coherence analysis,[33] but the modulation frequencies at 510 and 930 cm^{-1} likely correspond to C = C torsional and hydrogen out-of-plane (HOOP) deformations of a conjugated polyene, respectively.[34,35] The 170 cm^{-1} component is consistent with that observed in resonance Raman spectra for out-of-plane deformations of porphyrin macrocycles.[36]

The Chl components in the global models decay in 3.1 ps in both complexes (Table 1). Given the long lifetime observed for the Chl S_1 (Q_y) state in PCP, which permits Chl-to-Chl excitation energy transfer in a given PCP monomer and between PCP monomers in the wtPCP-Chl *a* trimer with time constants of 6.8 ps and 350 ps, respectively,[24,37,38] an assignment of the 3.1-ps decay component to vibrational cooling should be considered first, and the kinetic model incorporates this assignment by connecting the Chl and Chl′ compartments with a nonradiative decay step. Vibrational relaxation in metalloporphyrins is typically observed on the 3- to 10 ps timescale.[39] The decay of the Chl-positive signal here would principally involve a shift of the SE to longer wavelengths as the $v = 2$ or $v = 1$ population relaxes to establish a Boltzmann distribution at the temperature of the surroundings, leaving nearly all of the population at the Q_y $v = 0$ level. These findings indicate that

Table 1. Time constants for the excitation energy transfer and nonradiative processes after optical excitation of the per2,3 or per1 excitons in wtPCP-Chl *a* and rPCP-Chl *b*

	wtPCP-Chl *a*		rPCP-Chl *b*	
	Per2,3	Per1	Per2,3	Per1
$1/k_{p23p1}$	10 ± 3 fs	–	13 ± 2 fs	–
$1/k_{p1C}$	24 ± 1 fs	26 ± 2 fs	29 ± 2 fs	28 ± 4 fs
$1/k_{IC}$	3.2 ± 0.1 ps	2.9 ± 0.1 ps	3.1 ± 0.6 ps	3.2 ± 2.4 ps
$1/k_{2x}$	35 ± 6 fs	38 ± 3 fs	35 ± 4 fs	37 ± 1 fs
$1/k_{x1}$	3.7 ± 0.5 ps	3.6 ± 0.5 ps	3.7 ± 0.5 ps	3.5 ± 0.2 ps
$1/k_{xC}$	1.3 ± 0.2 ps	1.2 ± 0.5 ps	1.9 ± 0.3 ps	2.2 ± 0.3 ps
$1/k_{10*}$	17.5 ± 2.1 ps	18.1 ± 1.8 ps	17.3 ± 1.9 ps	18.0 ± 1.3 ps
$1/k_{0*0}$	27.2 ± 3.0 ps	30.0 ± 2.2 ps	28.4 ± 3.0 ps	29.1 ± 2.8 ps

vibrational cooling contributes to the rising signal amplitude observed at the Q_y v = 0 transition in previous work. Bautista et al.[20] observed a rising transient at 670 nm for the Q_y v = 0 transition in the wtPCP-Chl *a* complex with a 3.2-ps time constant that is consistent with this assignment.

The calculated extent of delocalization for the exciton states in PCP collapses during excitation transfer

A detailed analysis of the electronic structure of the chromophore cluster in PCP using natural transition orbitals (NTOs; hole → particle excitations)[17] is consistent with the conclusion made above that the delocalized excitation present initially after excitation of the peridinin excitons collapses as excitation energy progresses along the pathway to the Chl acceptor. Our previous NTO study of the excitations in PCP indicated that the per2 and per3 excitons are delocalized over three of the four peridinin molecules in a given PCP domain. The per1 exciton, however, has electron density extending over only two peridinin molecules and is centered mainly on peridinin 614 (Figure 1B). Per4, which is not optically populated by the laser spectrum in the present work, was also determined to be delocalized over only two peridinin molecules, mainly Per 612 and 611.[17] These previous quantum mechanics (QM)/molecular mechanics (MM) calculations of the peridinin excitation energies at the time-dependent density functional theory (TDDFT) level (500 nm, 493 nm, 476 nm, and 447 nm) reproduced very well the corresponding experimental values for S_0 (v = 0) → S_2 (v = 1) transitions in rPCP-Chl *b*(511 nm, 497 nm, 483 nm, and 453 nm), but they did not include the Chl *a* acceptor in the quantum region for the calculation of excitation energies and NTO analysis. However, here we can show that, when Chl *a* is included in the calculation, per1 is found to be delocalized principally over peridinin 614 and Chl *a* (Figure 7; Table 2).

Inclusion of Chl *a* in the calculation alters the exciton transition wavelengths by no more than 5 nm. However, because of the use of TDDFT, there is a significant spurious charge transfer (CT) character mixed into the longest wavelength allowed transitions when the multichromophoric region includes Chl *a*. To obtain a better description of the delocalized excited state density at the cost of accuracy for the transition wavelengths, we performed a calculation of the lowest-energy excitons at the configuration interaction with singles (CIS)/LACVP* level of theory for the PCP chromophore cluster. Indeed, at the CIS level of theory, we find that there is no CT character in the longest-wavelength transitions. Table 2 shows the principal contributions of NTOs to the lowest 10 energy states in the Franck-Condon region for the chromophore cluster in PCP. The transition wavelengths returned by the calculations are listed in Table 2 only to show the energy ordering of the excitons. It is well known that the CIS theory provides poor estimates for the gaps between energy levels, but the orbital contributions obtained from the NTO analysis are qualitatively correct.

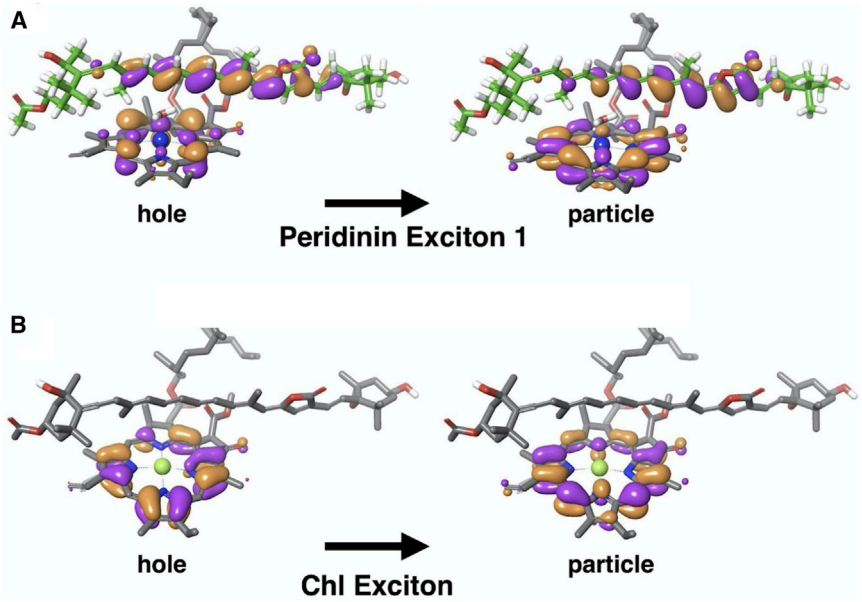

Figure 7. CIS calculations of natural transition orbitals (NTOs) in the wtPCP-Chl *a* complex
(A and B) NTOs for (A) the lowest-energy peridinin exciton, per1, and (B) the Chl *a* exciton. Only peridinin 614 and Chl *a*, the principal contributors to these excitons, are shown.

The results in Table 2 indicate that the per2, per3, and per1 exciton states in the PCP chromophore cluster contain significant delocalizations onto the Chl acceptor. As excitation is transferred down the pathway, however, the electron density focuses markedly. States 3 and 4, which correspond to the per2 and per3 excitons, contain 13% contributions from Chl *a* and the balance from two or three of the peridinin chromophores. Excitation transfer from per2,3 to the per1 exciton, state 2 in the Table 2, contracts the delocalized electron density to a single peridinin, peridinin 614 (75%), and the extent of delocalization onto the Chl *a* acceptor increases to 18%. The last step in the excitation transfer pathway involves trapping of excitation on the Chl acceptor and loss of any peridinin character; state 1, the lowest energy exciton in PCP, is entirely localized on Chl *a*. Note S6 and Figure S13 depict the electron density for each of the hole-particle excitations contributing to state 1. Only the largest of these (80%) is pictured in Figure 7.

DISCUSSION

Nonadiabatic mechanisms,[40] involving concerted vibrational and electronic motions, have been discussed in a number of previous studies of excitation energy transfer in photosynthetic light-harvesting systems. In this area, the work of Womick and Moran[41] on the isostructural phycobiliproteins allophycocyanin and *C*-phycocyanin from cyanobacteria first identified how vibronic resonance, matching of the energy gaps between the exciton energy levels by the vibrational quanta of the chromophores, can accelerate interexciton relaxation and enhance delocalization over a cluster of chromophores. Tiwari et al.[42] subsequently reported simulations indicating that vibronic resonance by weakly coupled anticorrelated vibrations promotes excitation energy transfer when the vibrations are delocalized over a pair of electronic chromophores. The excitation transfer mechanism in this situation is effectively an internal conversion between exciton potential surfaces arranged in a nested funnel. According to current thinking, the resonant vibrational modes serve as incoherent spectators with respect to the reaction coordinate for the internal conversion or excitation transfer process.[43]

Table 2. Contributions of NTOs to the lowest 10 energy states of the multichromophoric system, including peridinins (Per611, 612, 613, and 614 and Chl *a* in the QM region using the CIS/LACVP* level of theory

State	λ (nm)	Oscillatory strength	Hole-particle excitations[a]	Total % of excitation
1	562	0.3079	80.1% Chl *a* > Chl *a*, 15.1% Chl *a** > Chl *a**	95.2%
2	398	1.3604	74.8% Per614 > Per614, 17.8% Chl *a* > Chl *a*	92.6%
3	395	0.509	40.2% Chl *a* > Chl *a*, 30.5% Per611 > Per611, 13.2% Chl *a** > Chl *a**	83.9%
4	390	2.0425	31.6% Per611 > Per611, 22.1% Per614 > Per614, 13.6% Chl *a* > Chl *a*, 11.4% Per612 > Per612	78.6%
5	375	1.0524	41.4% Per612 > Per612, 40.7% Per613 > Per613	82.2%
6	363	9.2868	40.0% Per613 > Per613, 29.7% Per612 > Per612, 12.1% Per611 > Per611	81.9%
7	310	0.8992	58.0% Chl *a* > Chl *a*, 34.2% Chl *a** > Chl *a**	92.2%
8	308	0.4221	80.0% Chl *a* > Chl *a*, 14.1% Chl *a** > Chl *a**	94.1%
9	308	0.0822	94.2% Per614 > Chl-*a* (CT state)	94.2%
10	284	1.2735	51.8% Chl *a* > Chl *a*, 18.3% Per614 > Per614	70.1%

Only contributions larger than 10% are shown. CT, charge transfer.
[a]An asterisk indicates that there are two different hole-particle excitations on a given molecule.

One of the novel findings of the present work, is that the measured time constants from the global models for the transfers of excitation from per2,3 to per1 and then to the Chl acceptors in the PCP complexes are relatively insensitive to the changes in the donor-acceptor energy gaps that accompany replacement of the Chl *a* acceptors with Chl *b*. One might have expected to observe an even faster interexciton relaxation in rPCP-Chl *b* because of the near resonance of the per1 exciton with the Q_y v = 2 level of Chl *b* (Figure 1E). The results show, however, that the per2,3 to per1 and per1 to Chl steps are actually slowed in rPCP-Chl *b* but at most by a few femtoseconds from the values observed in wtPCP-Chl *a* (Table 1). It is possible that the rPCP-Chl *b* complex achieves this robustness by employing the v = 2 and v = 1 Chl levels as acceptors, but the 2DES spectra from rPCP-Chl *b* (Figure 3) do not develop a cross-peak like that observed in the spectra from wtPCP-Chl *a* in the v = 2 region (Figure 2); a weak cross-peak is noted, however, at the red edge of the spectrum, which correlates better with the shoulder of the v = 1 transition.

As mentioned in the Introduction, the question of whether the excitation transfer dynamics in PCP involve the strong electronic coupling regime associated with interexciton nonradiative processes[3] would seem to be answered by the global models of the 2DES spectra in the wtPCP-Chl *a* and rPCP-Chl *b* complexes. The time constants for excitation transfer along the pathway from the per2,3 exciton to the Chl acceptors are consistent with the strong coupling regime, even for the rate-limiting step from the per1 intermediate to the Chl acceptor (<30 fs; Table 2). Intriguingly, however, the PCP complexes clearly operate with a delicate balance of the electronic couplings between the chromophores and the system-bath couplings to the surrounding protein and solvent water medium. The 2DES spectra show that the delocalized character present initially over the peridinin-Chl cluster collapses with each step along the pathway and that a localized Chl acceptor is the product in less than 50 fs. This conclusion is well supported by the companion electronic structure calculations, which reveal that the per1 exciton is the key state retaining delocalization over the per614 peridinin (Figure 1B) and the structurally adjacent Chl acceptor. A consequence of this dynamic localization process is that the accompanying excitation transfer process is rendered irreversible; the Chl acceptor essentially traps the excitation energy at the end of the initially delocalized pathway.

Additional investigations will be required to fully understand the nonadiabatic mechanism that mediates the transfer of excitation in the wtPCP-Chl *a* and rPCP-Chl *b* complexes, but involvement of out-of-plane vibrations of the peridinin isoprenoid backbone should be considered. Because of its carbonyl substituent, peridinin has an ICT character that would contribute to stronger mixing with the Chl electronic states. The ICT character is enhanced by static out-of-plane deformations of the isoprenoid backbone, including those imposed on the peridinins by the binding sites in the chromophore cluster in PCP, but the torsional and pyramidal distortions that have been proposed to follow optical excitation to the S_2 state would result in even larger enhancements, even as bound in the chromophore cluster in PCP.[11] Accordingly, it is reasonable to propose that these peridinin vibrations play an important dynamic role in transfer of excitation to the Chl acceptors in PCP, but they are clearly also involved in the dynamic localization process that affords irreversibility. These findings raise the fascinating possibility that smart light-harvesting materials can be engineered to optimize their ability to capture the energy from solar photons by taking advantage of strong dynamic couplings to CT states.

EXPERIMENTAL PROCEDURES

Resource availability

Lead contact

Further information and requests for resources and reagents should be directed to and will be fulfilled by the lead contact, Warren F. Beck (beckw@msu.edu).

Materials availability

This study did not generate new unique reagents.

Data and code availability

The datasets supporting the current study have not been deposited in a public repository because, at present, a suitable one is not available, but they are available from the lead contact on request. All software codes used for data analysis are available commercially, but the scripts used during the work are available from the lead contact upon request.

Sample preparation

wtPCP-Chl *a* was isolated by Prof. Roger Hiller (Macquarie University) from *Amphidinium carterae* cells using a method published previously.[44] rPCP–Chl *b* was made with N-terminal domain PCP apoprotein expressed in *Escherichia coli* and reconstituted with peridinin and Chl *b* using procedures reported previously.[21]

Femtosecond spectroscopy

2DES experiments were performed with a newly constructed spectrometer employing a two-beam, pump-probe configuration with adaptive pulse shaping.[29] The pump and probe beams in the spectrometer were obtained from a noncollinear optical parametric amplifier that was pumped by the third harmonic of a 1.04-μm amplified Yb laser. The Supplemental experimental procedures and Note S1 provide additional details regarding the apparatus and the methods used to characterize the 15-fs pulses.

Excited state calculations

Calculations were carried out using Qsite[46] (Schrödinger Inc., release 2017-1) using the Poisson-Boltzmann finite (PBF) difference method[47] to treat solvent effects. CIS was used to compute the excited states of a multichromophoric QM/MM system. CIS/LACVP* model chemistry and the OPLSS-AA force field were used for the QM and MM regions, respectively.

SUPPLEMENTAL INFORMATION

Supplemental information can be found online at https://doi.org/10.1016/j.xcrp.2021.100380.

ACKNOWLEDGMENTS

This work was principally supported by the Photosynthetic Systems Program of the Chemical Sciences, Geosciences, and Biosciences Division, Office of Basic Energy Sciences, Office of Science, U.S. Department of Energy under award DE-SC0010847. Additional analyses in the laboratory of W.F.B. and on electronic structure in the laboratory of J.G. were supported by collaborative research grants from the Chemistry of Life Sciences Program of the U.S. National Science Foundation (CHE-1904700 and CHE-1904655, respectively). Work in the laboratory of H.A.F. was also supported by grants from the National Science Foundation (MCB-1243565) and the University of Connecticut Research Foundation. S.G. acknowledges support from the European Commission through Marie Sklodowska-Curie Actions (H2020-MSCA-IF-2018-841356). We thank Prof. Roger Hiller (Macquarie University) for the generous gifts of the WT PCP samples, peridinin, and the expression construct for the N-terminal domain apoprotein of PCP, which were required for the Chl *b* reconstitution procedure.

AUTHOR CONTRIBUTIONS

R.W.T., J.D.R., J.K.G. , and W.F.B. carried out the experiments and data analysis. M.J.G.-P. and J.A.G. provided the electronic structure calculations. H.A.F. and A.M.L. prepared samples. R.W.T., M.J.G.-P., J.K.G., S.G., J.K.G., and W.F.B. wrote the manuscript and supplemental information. The research plan was designed by W.F.B., H.A.F., and J.A.G. The overall project was directed by W.F.B.

DECLARATION OF INTERESTS

The authors declare no competing interests.

Received: November 16, 2020
Revised: February 8, 2021
Accepted: February 24, 2021
Published: March 17, 2021

REFERENCES

1. Blankenship, R.E. (2014). Molecular Mechanisms of Photosynthesis (John Wiley & Sons).
2. Ishizaki, A., and Fleming, G.R. (2012). Quantum Coherence in Photosynthetic Light Harvesting. Annu. Rev. Condens. Matter Phys. *3*, 333–361.
3. Chenu, A., and Scholes, G.D. (2015). Coherence in energy transfer and photosynthesis. Annu. Rev. Phys. Chem. *66*, 69–96.
4. Niedringhaus, A., Policht, V.R., Sechrist, R., Konar, A., Laible, P.D., Bocian, D.F., Holten, D., Kirmaier, C., and Ogilvie, J.P. (2018). Primary processes in the bacterial reaction center probed by two-dimensional electronic spectroscopy. Proc. Natl. Acad. Sci. USA *115*, 3563–3568.
5. Jumper, C.C., Anna, J.M., Stradomska, A., Schins, J., Myahkostupov, M., Prusakova, V., Oblinsky, D.G., Castellano, F.N., Knoester, J., and Scholes, G.D. (2014). Intramolecular radiationless transitions dominate exciton relaxation dynamics. Chem. Phys. Lett. *599*, 23–33.
6. Duan, H.-G., Prokhorenko, V.I., Cogdell, R.J., Ashraf, K., Stevens, A.L., Thorwart, M., and Miller, R.J.D. (2017). Nature does not rely on long-lived electronic quantum coherence for photosynthetic energy transfer. Proc. Natl. Acad. Sci. USA *114*, 8493–8498.
7. Beljonne, D., Curutchet, C., Scholes, G.D., and Silbey, R.J. (2009). Beyond Förster resonance energy transfer in biological and nanoscale systems. J. Phys. Chem. B *113*, 6583–6599.
8. Jonas, D.M. (2003). Two-dimensional femtosecond spectroscopy. Annu. Rev. Phys. Chem. *54*, 425–463.
9. Mimuro, M., Tamai, N., Ishimaru, T., and Yamazaki, I. (1990). Characteristic fluorescence components in photosynthetic pigment system of a marine dinoflagellate, *Protogonyaulax tamarensis*, and excitation energy flow among them. Studies by means of steady-state and time-resolved fluorescence spectroscopy. Biochim. Biophys. Acta Bioenergetics *1016*, 280–287.
10. Hofmann, E., Wrench, P.M., Sharples, F.P., Hiller, R.G., Welte, W., and Diederichs, K. (1996). Structural basis of light harvesting by carotenoids: peridinin-chlorophyll-protein from *Amphidinium carterae*. Science *272*, 1788–1791.
11. Ghosh, S., Bishop, M.M., Roscioli, J.D., LaFountain, A.M., Frank, H.A., and Beck, W.F. (2017). Excitation energy transfer by coherent and incoherent mechanisms in the peridinin–chlorophyll *a* protein. J. Phys. Chem. Lett. *8*, 463–469.

12. Roscioli, J.D., Ghosh, S., LaFountain, A.M., Frank, H.A., and Beck, W.F. (2017). Quantum Coherent Excitation Energy Transfer by Carotenoids in Photosynthetic Light Harvesting. J. Phys. Chem. Lett. *8*, 5141–5147.

13. Roscioli, J.D., Ghosh, S., LaFountain, A.M., Frank, H.A., and Beck, W.F. (2018). Structural Tuning of Quantum Decoherence and Coherent Energy Transfer in Photosynthetic Light Harvesting. J. Phys. Chem. Lett. *9*, 5071–5077.

14. Meneghin, E., Volpato, A., Cupellini, L., Bolzonello, L., Jurinovich, S., Mascoli, V., Carbonera, D., Mennucci, B., and Collini, E. (2018). Coherence in carotenoid-to-chlorophyll energy transfer. Nat. Commun. *9*, 3160.

15. Carbonera, D., Giacometti, G., Segre, U., Hofmann, E., and Hiller, R.G. (1999). Structure-based calculations of the optical spectra of the light-harvesting peridinin–chlorophyll–protein complexes from *Amphidinium carterae* and *Heterocapsa pygmaea*. J. Phys. Chem. B *103*, 6349–6356.

16. Andreussi, O., Knecht, S., Marian, C.M., Kongsted, J., and Mennucci, B. (2015). Carotenoids and light-harvesting: from DFT/MRCI to the Tamm-Dancoff approximation. J. Chem. Theory Comput. *11*, 655–666.

17. Guberman-Pfeffer, M.J., Greco, J.A., Birge, R.R., Frank, H.A., and Gascón, J.A. (2018). Light Harvesting by Equally Contributing Mechanisms in a Photosynthetic Antenna Protein. J. Phys. Chem. Lett. *9*, 563–568.

18. Zigmantas, D., Hiller, R.G., Sundstrom, V., and Polivka, T. (2002). Carotenoid to chlorophyll energy transfer in the peridinin-chlorophyll-*a*-protein complex involves an intramolecular charge transfer state. Proc. Natl. Acad. Sci. USA *99*, 16760–16765.

19. Kleima, F.J., Wendling, M., Hofmann, E., Peterman, E.J., van Grondelle, R., and van Amerongen, H. (2000). Peridinin chlorophyll *a* protein: relating structure and steady-state spectroscopy. Biochemistry *39*, 5184–5195.

20. Bautista, J.A., Hiller, R.G., Sharples, F.P., Gosztola, D., Wasielewski, M., and Frank, H.A. (1999). Singlet and Triplet Energy Transfer in the Peridinin−Chlorophyll *a*−Protein from *Amphidinium carterae*. J. Phys. Chem. A *103*, 2267–2273.

21. Miller, D.J., Catmull, J., Puskeiler, R., Tweedale, H., Sharples, F.P., and Hiller, R.G. (2005). Reconstitution of the peridinin-chlorophyll *a* protein (PCP): evidence for functional flexibility in chlorophyll binding. Photosynth. Res. *86*, 229–240.

22. Polívka, T., Pascher, T., Sundström, V., and Hiller, R.G. (2005). Tuning energy transfer in the peridinin-chlorophyll complex by reconstitution with different chlorophylls. Photosynth. Res. *86*, 217–227.

23. Schulte, T., Hiller, R.G., and Hofmann, E. (2010). X-ray structures of the peridinin-chlorophyll-protein reconstituted with different chlorophylls. FEBS Lett. *584*, 973–978.

24. Ilagan, R.P., Shima, S., Melkozernov, A., Lin, S., Blankenship, R.E., Sharples, F.P., Hiller, R.G., Birge, R.R., and Frank, H.A. (2004). Spectroscopic properties of the main-form and high-salt peridinin-chlorophyll a proteins from *Amphidinium carterae*. Biochemistry *43*, 1478–1487.

25. Guberman-Pfeffer, M.J., and Gascón, J.A. (2018). Carotenoid-Chlorophyll Interactions in a Photosynthetic Antenna Protein: A Supramolecular QM/MM Approach. Molecules *23*, 1420–3049.

26. Schulte, T., Niedzwiedzki, D.M., Birge, R.R., Hiller, R.G., Polívka, T., Hofmann, E., and Frank, H.A. (2009). Identification of a single peridinin sensing Chl-*a* excitation in reconstituted PCP by crystallography and spectroscopy. Proc. Natl. Acad. Sci. USA *106*, 20764–20769.

27. Kobayashi, M., Akiyama, M., Kano, H., and Kise, H. (2006). Spectroscopy and Structure Determination. In Chlorophylls and Bacteriochlorophylls: Biochemistry, Biophysics, Functions and Applications, B. Grimm, R.J. Porra, W. Rüdiger, and H. Scheer, eds. (Springer), pp. 79–94.

28. Reimers, J.R., Cai, Z.L., Kobayashi, R., Rätsep, M., Freiberg, A., and Krausz, E. (2013). Assignment of the Q-bands of the chlorophylls: coherence loss via Q_x - Q_y mixing. Sci. Rep. *3*, 2761.

29. Shim, S.H., and Zanni, M.T. (2009). How to turn your pump-probe instrument into a multidimensional spectrometer: 2D IR and Vis spectroscopies via pulse shaping. Phys. Chem. Chem. Phys. *11*, 748–761.

30. van Stokkum, I.H., Larsen, D.S., and van Grondelle, R. (2004). Global and target analysis of time-resolved spectra. Biochim. Biophys. Acta *1657*, 82–104.

31. Pullerits, T., Chachisvilis, M., Jones, M.R., Hunter, C.N., and Sundström, V. (1994). Exciton dynamics in the light-harvesting complexes of *Rhodobacter sphaeroides*. Chem. Phys. Lett. *224*, 355–365.

32. Scholes, G.D., and Smyth, C. (2014). Perspective: Detecting and measuring exciton delocalization in photosynthetic light harvesting. J. Chem. Phys. *140*, 110901.

33. Thyrhaug, E., Bogh, S.A., Carro-Temboury, M.R., Madsen, C.S., Vosch, T., and Zigmantas, D. (2017). Ultrafast coherence transfer in DNA-templated silver nanoclusters. Nat. Commun. *8*, 15577.

34. Lin, S.W., Groesbeek, M., van der Hoef, I., Verdegem, P., Lugtenburg, J., and Mathies, R.A. (1998). Vibrational assignment of torsional normal modes of rhodopsin: probing excited-state isomerization dynamics along the reactive C11=C12 torsion coordinate. J. Phys. Chem. B *102*, 2787–2806.

35. Llansola-Portoles, M.J., Pascal, A.A., and Robert, B. (2017). Electronic and vibrational properties of carotenoids: from *in vitro* to *in vivo*. J. R. Soc. Interface *14*, 20170504.

36. Diers, J.R., Zhu, Y., Blankenship, R.E., and Bocian, D.F. (1996). Q_y-excitation resonance Raman spectra of chlorophyll *a* and bacteriochlorophyll *c/d* aggregates. Effects of peripheral substituents on the low-frequency vibrational characteristics. J. Phys. Chem. *100*, 8573–8579.

37. Kleima, F.J., Hofmann, E., Gobets, B., van Stokkum, I.H., van Grondelle, R., Diederichs, K., and van Amerongen, H. (2000). Förster excitation energy transfer in peridinin-chlorophyll-*a*-protein. Biophys. J. *78*, 344–353.

38. Polívka, T., Hiller, R.G., and Frank, H.A. (2007). Spectroscopy of the peridinin-chlorophyll-*a* protein: insight into light-harvesting strategy of marine algae. Arch. Biochem. Biophys. *458*, 111–120.

39. Rodriguez, J., and Holten, D. (1989). Ultrafast vibrational dynamics of a photoexcited metalloporphyrin. J. Chem. Phys. *91*, 3525–3531.

40. Curchod, B.F.E., and Martínez, T.J. (2018). Ab Initio Nonadiabatic Quantum Molecular Dynamics. Chem. Rev. *118*, 3305–3336.

41. Womick, J.M., and Moran, A.M. (2009). Exciton coherence and energy transport in the light-harvesting dimers of allophycocyanin. J. Phys. Chem. B *113*, 15747–15759.

42. Tiwari, V., Peters, W.K., and Jonas, D.M. (2013). Electronic resonance with anticorrelated pigment vibrations drives photosynthetic energy transfer outside the adiabatic framework. Proc. Natl. Acad. Sci. USA *110*, 1203–1208.

43. Jumper, C.C., Rafiq, S., Wang, S., and Scholes, G.D. (2018). From coherent to vibronic light harvesting in photosynthesis. Curr. Opin. Chem. Biol. *47*, 39–46.

44. Sharples, F.P., Wrench, P.M., Ou, K., and Hiller, R.G. (1996). Two distinct forms of the peridinin-chlorophyll *a*-protein from *Amphidinium carterae*. Biochim. Biophys. Acta *1276*, 117–123.

46. Murphy, R.B., Philipp, D.M., and Friesner, R.A. (2000). A mixed quantum mechanics/molecular mechanics (QM/MM) method for large-scale modeling of chemistry in protein environments. J. Comput. Chem. *21*, 1442–1457.

47. Tannor, D.J., Marten, B., Murphy, R., Friesner, R.A., Sitkoff, D., Nicholls, A., Honig, B., Ringnalda, M., and Goddard, W.A. (1994). Accurate First Principles Calculation of Molecular Charge Distributions and Solvation Energies from Ab Initio Quantum Mechanics and Continuum Dielectric Theory. J. Am. Chem. Soc. *116*, 11875–11882.